Surface pressure and wind stress effects on sea level change estimations from TOPEX/Poseidon satellite altimetry in the Mediterranean Sea

Sylvain Mangiarotti, F. Lyard

Surface Pressure and Wind Stress Effects on Sea Level Change Estimations from TOPEX/Poseidon Satellite Altimetry in the Mediterranean Sea

S. MANGIAROTTI AND F. LYARD

POC-LEGOS-CNRS, UMR5566/CNRS-IRD-UPS-CNES, Toulouse, France

(Manuscript received 16 May 2005, in final form 7 December 2006)

ABSTRACT

Using the classical inverse barometer (IB) correction and the Modèle d'Onde de Gravité à 2 Dimensions (MOG2D) barotropic model in the Mediterranean Sea during the 1993–2002 period, it is shown that surface pressure and wind stress forcing significantly contribute to sea level elevation variations observed with Ocean Topography Experiment (TOPEX)/Poseidon (T/P) satellite altimetry. The barotropic model allows the authors to estimate the high-frequency atmospheric ocean response that is aliased into the altimetric sea level. Applying the model barotropic correction allows them to reduce the T/P standard deviation by a mean of 21% over the whole basin, whereas the classical IB correction reduces the standard deviation by only 16%. The trend in sea level rise is also strongly affected due to the aliasing effect, especially when short periods are considered. On a 3-yr period, the correction associated with either of these two models can reach 10–12 mm yr^{-1}. Applying the barotropic model correction rather than the IB correction can also affect the linear trend estimations by more than 6–7 mm yr^{-1}. For a 9-yr window, the IB/MOG2D correction can contribute 1.8–2 mm yr^{-1} in magnitude. The local corrected linear trends confirm the previous analysis pattern but on a local scale, with the linear trend magnitudes reaching values between −24 and +29 mm yr^{-1}.

1. Introduction

Sea level elevation (SLE) is one of the major indicators of climate evolution. Several processes can affect SLE on the time scale considered here (3–9 yr) in the Mediterranean Sea. Among the possible sources causing SLE variations are 1) temperature variations, in deep water (as it was observed by Béthoux et al. 1990, 1998; Mangiarotti 2003) and in surface water (Cazenave et al. 2001; Mangiarotti 2003), which contribute to the water column dilatation and contraction. 2) Salinity variations may also have a significant contribution in the Mediterranean basin as was initially suggested by Tsimplis and Baker (2000). Other processes may come from 3) mass exchanges through straits (Ross et al. 2000) or via the atmosphere (Béthoux and Gentili 1999); 4) ocean changing circulation (Pinardi and Masetti 2000) including current and gyre displacements due to flux instabilities (Ayoub et al. 1998; Larnicol et al. 2002); 5) ocean tides; and, finally, 6) surface pressure and wind stress.

We consider here the period January 1993 to February 2002 over which the most accurate SLE measurements in the open ocean come from Ocean Topography Experiment (TOPEX)/Poseidon (T/P) satellite altimetry. The precision associated with an individual measurement is estimated around 4.1 cm (Chelton et al. 2001). However, the accuracy of these measurements is affected by the 10-day repeat sampling of this instrument, causing an aliasing effect in the analysis of high-frequency sea level variations. In this paper, therefore, frequencies corresponding to periods shorter than 20 days will be considered as high frequency. The aliasing effects are especially well known from tidal analysis (Le Provost 2001). However, tides are not the only high-frequency signal affected by this aliasing effect. On a global scale, the power spectrum of the atmospherically forced signal is most energetic at periods less than 10 days (Hirose et al. 2001), and it will thus contribute a strong aliasing effect in the SLE estimation. The Mediterranean Sea, being a

Corresponding author address: S. Mangiarotti, POC-LEGOS-CNRS, UMR5566/CNRS-IRD-UPS-CNES, 18, Avenue Edouard Belin, 31401 Toulouse, France.
E-mail: mangiaro@notos.cst.cnes.fr

DOI: 10.1175/2006JTECHO419.1

semienclosed basin, has a tidal amplitude that does not exceed 0.1 m, except in the Adriatic Sea and in the Gulf of Gabes (East Tunisian coast) where it can reach approximately 0.5 and 1 m, respectively. High-frequency SLE variations are thus mainly dominated by the atmospheric effects of wind and pressure. This makes this domain particularly suitable for a study dedicated to the ocean response to wind- and pressure-driven processes. The atmospheric pressure together with wind stress will be generically called atmospheric loading for our purposes.

It is well known that the inverse barometer (IB) correction does not work well in semienclosed regions such as the Mediterranean Sea (Garrett 1983; Ducet et al. 1999; Tsimplis and Vlahakis 1994; Tsimplis et al. 2004). Indeed, the sea level can respond to the mean pressure over an enclosed basin only if an adjustment through the straits is made possible. The response thus highly depends on the water flux at the straits. Therefore, two high-frequency corrections will be considered for this study: 1) the classical IB model, which takes into account the static SLE response to surface atmospheric pressure loading, and 2) a barotropic model [we used here the Modèle d'Onde de Gravité à 2 Dimensions (MOG2D)] able to estimate the ocean response to both surface pressure and wind forcing.

In this paper we will focus on the atmospherically forced trends ranging from 3- to 9-yr windows that integrate all the frequencies lower than the observation window. Previous SLE linear trend analyses of satellite altimetry have been concerned with larger spatial scale variations during the 1990s. As it was shown by Cazenave et al. (2001) and Fenoglio-Marc (2002), the Mediterranean Sea trends behavior is clearly inhomogeneous, with a moderate sea level rise in the western basin and a strong sea level rise in the eastern basin, except in the Ionian Sea where a marked sea level decrease is observed. In this paper, the analysis will concentrate on more localized behavior (at a tens of kilometer scale) along the TOPEX/Poseidon ground tracks.

In the second section of this paper, a detailed description of the altimetry preprocessing and data preparation is given as well as a description of the MOG2D model and of the IB model used for this study. Results and discussions are presented in the third section; the models' skill is discussed first. The aliasing effect is then illustrated using an example of undersampling of an hourly tide gauge station analysis. We then consider the aliasing effect of the T/P data sampling, and finally provide a statistical estimation of its magnitude. Conclusions are then presented in section 4.

2. Method

a. Data preprocessing and preparation

We have used T/P data from the AVISO/Altimetry Project over the period January 1993 to February 2002, with the National Aeronautics and Space Administration (NASA) Goddard orbits. The following corrections have been applied: the ionosphere correction C_{iono} (all the symbols are summarized in Table 1) from the bifrequency altimetric measurement; the wet and dry tropospheric corrections C_{tropo} deduced respectively from radiometer measurements and from European Centre for Medium-Range Weather Forecasts (ECMWF) pressure; the sea state bias C_{ssb} from the BM4 algorithm (Gaspar et al. 1994); C_{tides}, the solid earth, polar, and ocean tides respectively from Cartwright and Tayler (1971), Cartwright and Edden (1973), and Whar (1985); and the FES99 model (Lefèvre 2000) and the ocean loading tides from the CSR3.0 model (Eanes and Bettadpur 1995). A geoid correction $C_{\text{JGM-3}}$ is applied from Joint Gravity Model 3 (JGM-3; Tapley et al. 1996) in order to remove the large wavelength component of the geoid. Instrumental corrections C_{TMR} and C_{alti} are also applied in order to take into account microwave radiometer drift and altimeter bias (see appendix A).

The local sea level elevation is then computed as follows:

$$h = h_{\text{obs}} - (C_{\text{iono}} + C_{\text{tropo}} + C_{\text{ssb}} + C_{\text{tides}} + C_{\text{JGM-3}} + C_{\text{TMR}} + C_{\text{alti}}), \quad (1)$$

where h_{obs} is the SLE estimate before corrections. Three cases of the IB correction are then considered, as follows:

$$h_\gamma = h - \mathrm{C}_\gamma, \quad (2)$$

with 1) $C_\gamma = C_0 = 0$ when no IB correction is applied; 2) $C_\gamma = C_{\text{IB}}$ when the classical IB correction is applied; and 3) $C_\gamma = C_{\text{MOG2D}}$ when the MOG2D model-derived correction is applied.

The along-track third-degree polynomial mean sea surface $M(\lambda, \varphi)$ is computed and subtracted from the data. The resulting anomalies are then spatially averaged in 0.2° boxes providing 10-day macromeasurements time series $\overline{h}_\gamma(t, \lambda, \varphi)$ of sea level anomalies (see appendix B for details).

A linear trend estimate $\hat{T}_\gamma$ is computed simultaneously with the annual cycle for each macromeasurement time series using a classical least squares method. The linear trend corrections associated with the classical IB and the MOG2D model-derived corrections are defined as

TABLE 1. Symbols used.

	Symbols
Lat	λ
Lon	φ
SLE estimate before corrections	h_{obs}
SLE estimate after corrections (except surface load)	h
Correction index (0, IB or MOG2D)	γ
Correction difference index (IB, MOG2D, wind) for (IB-noIB, MOG2D-noIB, MOG2D-IB) respect	$\delta\gamma$
SLE estimate after corrections (including surface load correction γ)	h_γ
Along-track mean sea surface	M
Sea level anomaly	$\hat{h}_\gamma$
No. of data available in a 0.2° of latitude box at one date	N
Macromeasurements sea level anomaly	$\overline{h}_\gamma$
Ionospheric correction	C_{iono}
Tropospheric corrections	C_{tropo}
Sea state bias correction	C_{ssb}
Solid earth polar and ocean tides corrections and ocean loading tides correction	C_{tides}
Large wavelength geoid correction	$C_{\text{JGM-3}}$
Instrumental radiometer correction	C_{TMR}
Altimeter bias correction	C_{alti}
Atmosphere loading correction	C_γ
Linear trend estimate based on data including surface load correction γ	$\hat{T}_\gamma$
Linear trend estimates based on perturbed data series	T_1, T_2
Linear trend correction associated with correction γ	$\delta\hat{T}_\gamma$
Linear trend correction due to wind and nonlinear dynamics	$\delta\hat{T}_{\text{wind}}$
Linear trend estimate error	ε
Time start of the window	τ
Linear trend estimate based on an L time window at date τ	$\hat{T}_\gamma^L$
Linear trend correction estimate based on an L time window at date τ	$\delta\hat{T}_\gamma^L$
Linear trend correction estimate associated with wind correction based on an L time window at date τ	$\delta\hat{T}_{\text{wind}}^L$
Mean max index (90% probability) of linear trend estimates	$\overline{\chi}_\gamma$
Mean max index (90%probability) of linear trend correction estimates	$\overline{\chi}_{\delta\gamma}$

$$\delta\hat{T}_{\text{IB}} = \hat{T}_0 - \hat{T}_{\text{IB}} \quad \text{and} \tag{3}$$

$$\delta\hat{T}_{\text{MOG2D}} = \hat{T}_0 - \hat{T}_{\text{MOG2D}}, \tag{4}$$

respectively, where $\hat{T}_0$ is the linear trend computed from the time series not corrected for any IB correction. The trend correction estimates $\delta\hat{T}_{\text{wind}}$ associated with the wind contribution is defined as follows:

$$\delta\hat{T}_{\text{wind}} = \hat{T}_{\text{MOG2D}} - \hat{T}_{\text{IB}}. \tag{5}$$

Because of the shortness of the time series, errors associated with these trend estimations are computed using a perturbation method rather than a classical formal one (see appendix C).

To study the convergence of the linear trend estimates as a function of the window length, several window lengths have been considered. For a given window length L, the linear trends and linear trend corrections are estimated from each macromeasurement series and at different starting times τ with a 1-month time step. Linear trends $\hat{T}_\gamma^L(\tau, \lambda, \varphi)$ are estimated in three cases: $\hat{T}_0^L(\tau, \lambda, \varphi)$, when no IB is applied; $\hat{T}_{\text{IB}}^L(\tau, \lambda, \varphi)$, when the IB correction is applied; and $\hat{T}_{\text{MOG2D}}^L(\tau, \lambda, \varphi)$, when the MOG2D correction is applied. The linear trend corrections $\delta\hat{T}_\gamma^L(\tau, \lambda, \varphi)$ are also estimated: $\delta\hat{T}_{IB}^L(\tau, \lambda, \varphi)$ is the linear trend correction associated with the IB correction, $\delta T_{MOG2D}^L(\tau, \lambda, \varphi)$ is the linear trend correction associated with the MOG2D correction, and $\delta\hat{T}_{\text{wind}}^L(\tau, \lambda, \varphi)$ is the linear trend correction associated with the difference between the MOG2D correction and the IB correction, and is related to the wind contribution.

We need an index able to represent at the same time a spatiotemporal mean behavior of the linear trends and their dispersion at a given window length L. Therefore, we define an index $\overline{\chi}_\gamma$ such that 90% of the estimated trends $\hat{T}_\gamma^L$ are lower than this index. Those trend estimates $\hat{T}_\gamma^L$ are considered for all time starts and all geographic positions. To define this index we thus use between 892 and 6244 trend values depending on the window length L considered (between 3 to 9 yr, respectively). We formally express this definition with the empirical probability $\hat{P}$:

$$\hat{\Pr}[\hat{T}_\gamma^L \leq \overline{\chi}_\gamma(L)] = 0.9. \tag{6}$$

In the same way, the other index $\overline{\chi}_{\delta\gamma}$ concerns the linear trend corrections $\delta\hat{T}^L_\gamma$:

$$\hat{\Pr}[\delta\hat{T}^L_\gamma \leq \overline{\chi}_{\delta\gamma}(L)] = 0.9. \quad (7)$$

These indices have been computed for window lengths L of 3 to 9 yr with a 1-yr time step and will be used in section 3d.

b. Model

1) MOG2D BAROTROPIC MODEL

MOG2D is a barotropic, time-stepping, nonlinear model, based on Lynch and Gray (1979), which has been developed at Laboratoire d'Etudes en Géophysique et Océanographie Spatiales (LEGOS), France. It is based on a wave equation formulation and the nonconservative momentum equations (Carrère and Lyard 2003; Carrère 2004). Forcing terms include the atmospheric surface pressure and wind stress. One of the most interesting aspects of this model is its finite-element spatial discretization (Lagrange P1-P1 type) allowing us to increase the resolution in coastal areas and over steep topographic regions. In this application, the Mediterranean-MOG2D grid size varies from 40 km over the deep ocean basins topography to nearly 2 km near the coastal areas. A subcycling time scheme allows us to adapt the time step dynamically and locally in order to control the model stability instead of tuning the horizontal viscosity terms.

The meteorological forcing fields are extracted from the ECMWF analysis (Cartesian grid products). The spatial resolution changed in 1998 from $1.125° \times 1.125°$ to $0.5° \times 0.5°$. This is rather a low spatial resolution for the period prior to 1998 when considering the coastal dynamics, and higher-resolution products are available from the national meteorological agencies. It was decided, however, to maintain the atmospheric forcing homogeneity in the framework of this study, so we have adopted ECMWF for the entire period. The temporal resolution of the ECMWF generic product is 6 h. As a consequence, the dynamics with periods equal or less than 12 h are misrepresented in the atmospheric forcing and hence in the model simulation. The wind stress is computed from wind speed through the classical bulk formula from Hellereman and Rosenstein (1983), in which the temperature difference between the ocean surface and the atmosphere is assumed to be zero. The Atlantic open boundary conditions are taken from the IB approximation through a radiative condition (characteristics method). Nine years of model simulations have been run between January 1993 and February 2002.

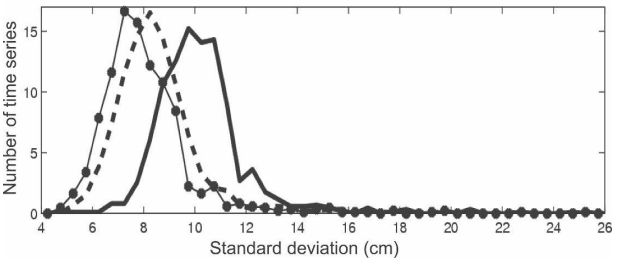

FIG. 1. Distribution of the time series std dev (cm) of SLE time series for the period 1993–2002 with no atmospheric loading correction (solid line), with the IB correction applied (dash line), and with the MOG2D correction applied (points line).

2) IB MODEL

The IB model is based on an approximation that assumes a static oceanic response to the atmospheric pressure loading (Fu and Pihos 1994), and totally ignores the wind effects. Its validity strongly depends on the basin considered and on the temporal and spatial scales considered (Tsimplis and Vlahakis 1994; Ducet et al. 1999; Tsimplis et al. 2004). The local IB is computed from the ECMWF sea level atmospheric pressure field corrected from its average over the global ocean (to insure global ocean mass conservation) as follows:

$$C_{\mathrm{IB}} = -\frac{P_a - \overline{P}_a}{\rho g}, \quad (8)$$

where P_a is the surface atmospheric pressure, $\overline{P}_a$ the averaged of the P_a over the whole ocean, ρ the averaged ocean density, and g the acceleration of gravity. This correction is dominated by an annual cycle of about ± 1 mb around 1011 mb.

3. Results and discussion

a. The model's skill

Atmospheric loading strongly influences SLE at the spatiotemporal scales considered here. For each along track computed time series, we have calculated standard deviation statistics for three cases: 1) with no atmospheric loading correction applied; 2) with the IB correction applied; and 3) with the MOG2D correction applied. The resulting distributions are given in Fig. 1.

When no atmospheric loading correction is applied, the standard deviation of the time series varies between 8 and 12 cm, with a mean value around 10 cm for the entire basin (Fig. 2a). High values (from 12 to 20 cm) can be found in some regions such as in the southwest of Crete where a strong baroclinic ocean signal associated with the Ierapetra gyre is well known (Pinardi and Masetti 2000; Larnicol et al. 2002); in the Alborian Ba-

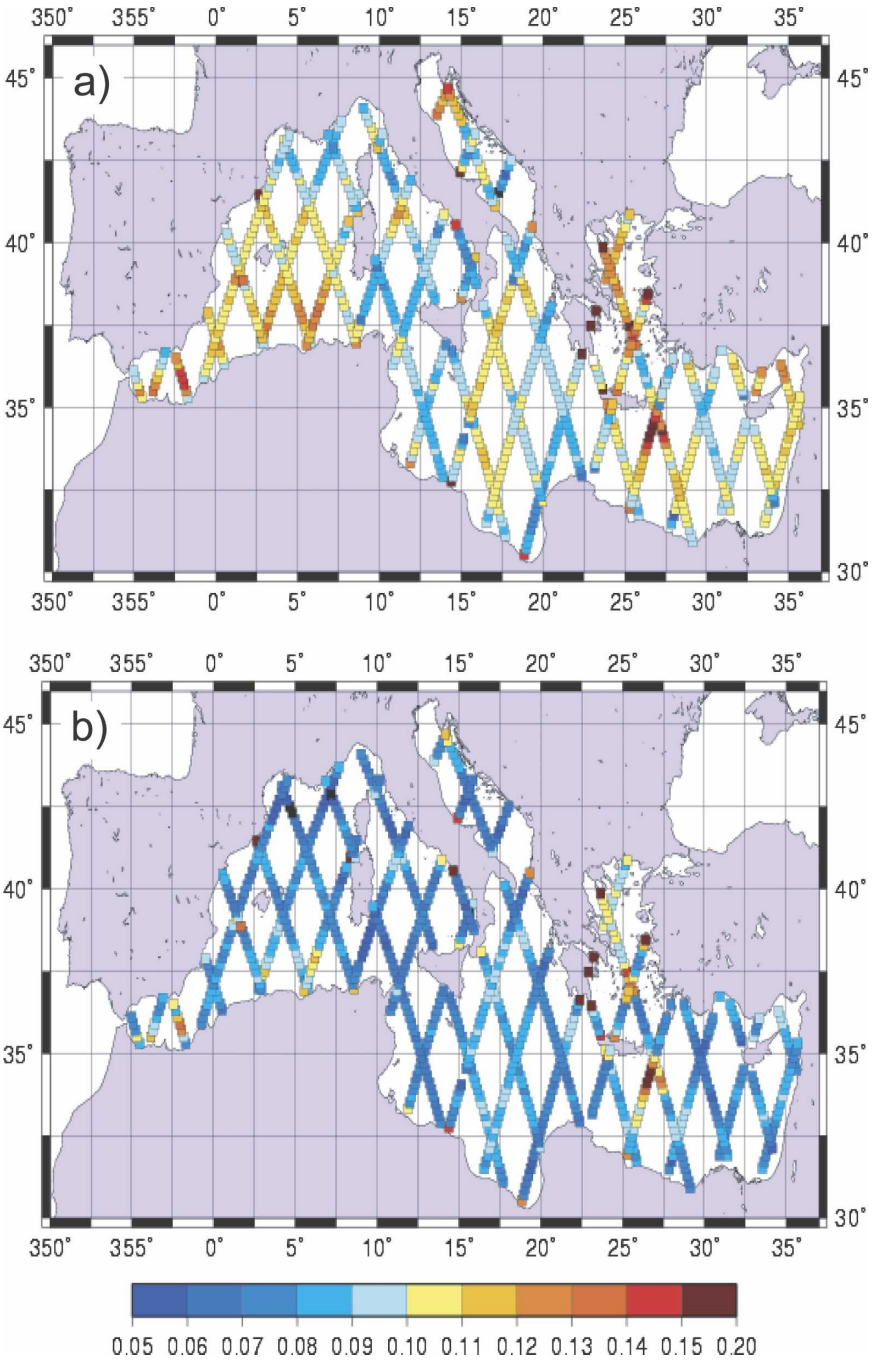

FIG. 2. Along-track T/P SLE std dev (m) on the period 1993–2002: (a) with no atmospheric loading correction applied and (b) with the MOG2D correction applied.

sin where a strong signal has been identified (Larnicol et al. 2002), which may come from the varying inflow/outflow through the Gibraltar Straits; along the Algerian coast where instabilities of the Algerian current form propagating eddies and meanders take place (Ayoub et al. 1998); in the northern Adriatic Sea where the strong mechanical wind forcing is well documented (Artegiani et al. 1997); and also at the end points of the tracks along the coastline where altimetric measurements accuracy is degraded. This coastal degradation mainly affects the radiometer measurement (used for the wet troposphere correction), which extends over the footprint size of 20-km radius. The altimetric measurement itself may also be contaminated but also be-

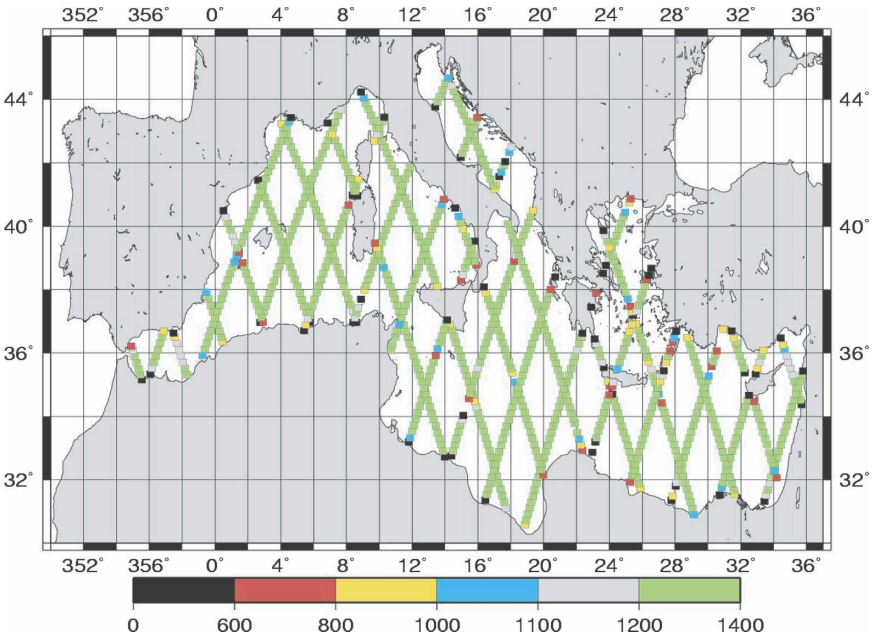

FIG. 3. Number of individual T/P measurements for each along-track zone.

comes saturated when the footprint touches the coast (its backscatter strongly depends on the sea state, its footprint ranges between 2- and 5-km radius). The number of reliable measurements is thus strongly diminished in the coastal region as shown in Fig. 3.

The MOG2D model-derived correction allows us to reduce the standard deviation by 21%, giving a mean standard deviation of 8.1 cm. This reduction is especially strong the in north Adriatic Sea where the wind action has a strong influence, but also in the Ionian Sea, in the Aegean Sea, in the Alborian Basin, and along the Algerian coast. Minimal standard deviation values are observed in the Gulf of Lion (where standard deviation magnitudes are less than 5 cm at several points) and do not exceed 9 cm over the entire basin (Fig. 2b). Higher values are observed in the Ionian and Aegean Seas (but do not exceed 10 and 11 cm, respectively). By contrast, regions with a strong baroclinic signal are even more apparent, especially in the Ierapetra gyre and in the Alborian Sea and also in coastal areas with complex bathymetry, such as the Aegean Sea.

The correction suggested by the IB model allows us to reduce the standard deviation by around 16% only (5% less than with the barotropic correction), lowering the mean standard deviation to 8.5 cm, and with most of the values ranging between 6 and 10 cm (not shown). Exceptions are encountered in the Ionian Sea, where values remain between 7 and 11 cm (due to the strong mesoscale ocean dynamics) and also in the regions where a strong oceanographic signal has already been described: in the Alborian Sea, along the Algerian current, in the Ierapetra gyre, and in the Aegean Sea. Along the continental shelf, degraded measurements remain with a high standard deviation.

b. *Linear trend estimates*

Linear trend estimates $\hat{T}_\alpha$ have been computed from the macromeasurements time series for the whole Mediterranean basin over the period January 1993–February 2002. The result (computed with the MOG2D correction applied) is shown in Fig. 4a.

Most of the linear trends vary between -20 and 24 mm yr^{-1}, except at three points located in the Ionian Sea and at three other points located in the Ierapetra gyre (Levantine basin). The basin-average sea level rise is globally positive (with a mean value of 3.5 ± 0.3 mm yr^{-1}), although the local behavior varies from one basin to another as was already noted (over shorter time periods) by Cazenave et al. (2001) and Fenoglio-Marc (2002). However, although the window considered here is longer than the one used by these previous authors, the values found here are slightly higher (the trends convergence as a function of the window length shown in Fig. 8 would suggest the contrary). The reason might be that here the estimations were calculated locally along the track, and no spatial smoothing was applied to the data. A rather homogeneous basin-scale behavior can be noticed with a moderate rise in the western basin (local values between -4.5 to 8.5 mm yr^{-1}, and 11 mm yr^{-1} at the junction between the Alborian Sea and

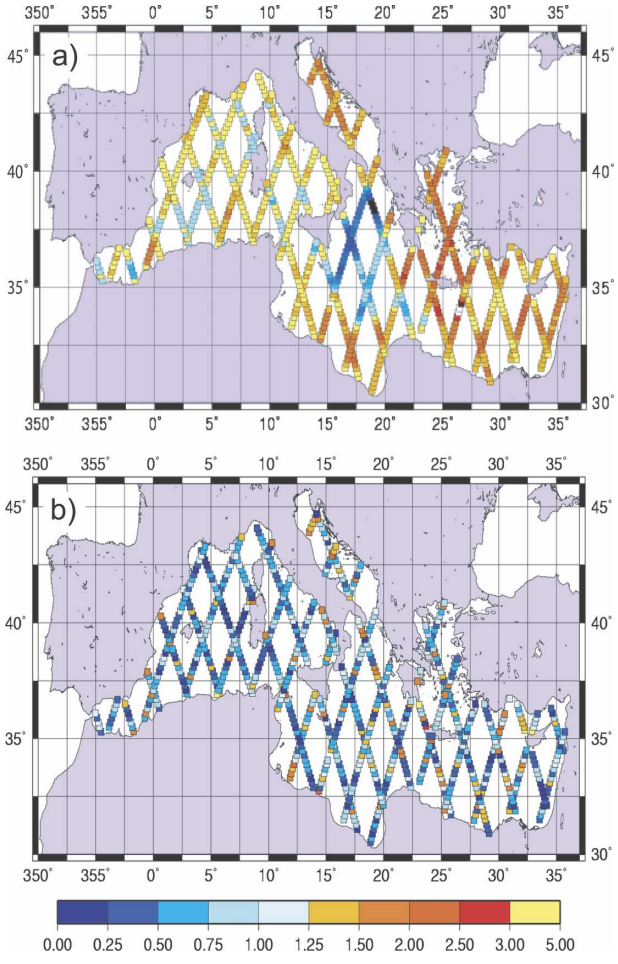

FIG. 4. (a) SLE linear trend estimation (mm yr^{-1}) over the Mediterranean Sea (1993–2002 period) from T/P data corrected with the MOG2D model. (b) Associated errors (mm yr^{-1}) that are lower than 2 mm yr^{-1} on the average.

the Algero-Provençal basin), a strong rise in the Adriatic Sea (from 4 to 14 mm yr^{-1}), in the Aegean Sea (from 8 to 17 mm yr^{-1} except for a few localized points), and also in the western part of the Levantine basin where values can exceed 24 mm yr^{-1} (reaching 29 mm yr^{-1} in the Ierapetra gyre) whereas in the eastern side these values are much more moderate (from 0 to 12 mm yr^{-1}). In the Ionian Sea, very contrasting trends are observed, with a moderate rise in the south (from 0 to 12 mm yr^{-1}), and a very strong decrease in the north (reaching locally -24 mm yr^{-1}). Error estimates associated with these trends are shown in Fig. 4b. Linear trends error estimates do not exceed 5 mm yr^{-1} and are generally less than 1.5 mm yr^{-1}. The strongest values are often located in coastal areas and in shallow bathymetric regions such as the Gulf of Gabes and in the north Adriatic Sea.

c. *An experimental characterization of the aliasing for linear trends estimation*

We can estimate the aliasing effect that would influence the linear trend for a typical T/P sampling scenario using an hourly sampled dataset. We have used the hourly Toulon tide gauge data over the period 1993–2000. These hourly data are subsampled at a 10-day period, and we vary the starting time by steps of 2 h over the first 10 days to simulate the phase difference. The linear trend is then estimated for each of these resampled time series (Fig. 5a). The same resampling and linear trend analysis has been performed for both atmospheric loading corrections (IB and MOG2D); the resulting curves are shown in Fig. 5a. It should be remembered that the IB and MOG2D model have a zero basin-scale trend. This could signify that the nonzero mean trends calculated from the IB and model-derived correction do not come from a model drift, but rather show a local physical behavior. Similar patterns are observed in these three signals, underlining the strong influence of atmospheric loading for linear trend estimation due to the aliasing effect.

If the atmospheric loading corrections are then applied to our tide gauge time series before the 10-day subsampling, the resulting shape of the curve is clearly smoothed (Fig. 5b), which confirms the atmospheric origin of this aliased signal. Finally, in terms of statistical analysis (Table 2), the IB and the MOG2D correction both reduce the dispersion of the linear trend distribution, improve the symmetry of the resulting distribution (skewness values nearer to zero), and accentuate its coherence (kurtosis closer to 3). This shows that when applying the IB and especially the MOG2D correction, the dependence on the phase sampling becomes smaller, and the undersampling effect is clearly reduced.

This experiment clearly reveals that an accurate estimation of the linear trend cannot be obtained from an aliased series such as T/P without first applying an atmospheric loading correction. Moreover a full wind-pressure dynamical effect correction, as provided by the MOG2D model, is more efficient than the IB correction.

d. *Atmospheric loading contribution to the linear trend estimation*

As shown previously the atmospheric loading signal is a significant contribution, which, through an important aliasing effect, will strongly contaminate the trend estimations. To estimate the contribution of atmospheric loading on linear trend estimation from T/P, linear trends have been estimated three ways: 1) with

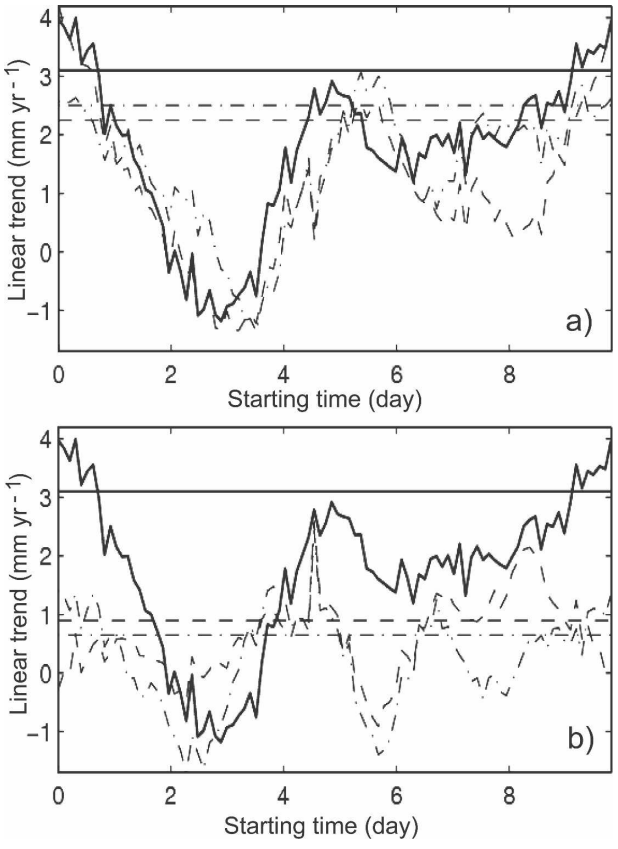

FIG. 5. Linear trend estimations (mm yr^{-1}) of the 10-day subsampled tide gauge data, atmospheric load correction data, and corrected tide gauge data as a function of the starting time (days). (a) Linear trend from the tide gauge with no IB correction (solid line), the IB correction only (dashed line), the MOG2D correction only (dashed–dotted line). Horizontal lines denote the mean linear trend from the Toulon hourly tide gauge data (plain line), from the IB correction only (dashed line) and from the MOG2D correction only (dashed–dotted line). (b) Linear trends from tide gauge: with no atmospheric loading correction (plain line), with the IB correction (dashed line), and with the MOG2D correction (dashed–dotted line). Horizontal lines denote the mean linear trend from the Toulon hourly tide gauge data (solid line), from the Toulon hourly tide gauge data corrected with the IB correction (dashed line), and from the Toulon hourly tide gauge data corrected with the MOG2D correction (dashed–dotted line).

no atmospheric loading correction applied; 2) with the IB correction applied; and 3) with the MOG2D correction applied. The two corrected cases $\hat{T}_{\mathrm{IB}}$ and $\hat{T}_{\mathrm{MOG2D}}$ have been compared to the noncorrected one $\hat{T}_0$. Resulting linear trend differences $\delta\hat{T}_{\mathrm{IB}}$ and $\delta\hat{T}_{\mathrm{MOG2D}}$ are respectively called IB trend correction and MOG2D trend correction and are shown in Fig. 6. Note, however, that correcting for the atmospheric loading response will not only correct the aliasing effect, but it will also remove the trend and the low-frequency signal associated with atmospheric pressure (and wind stress

TABLE 2. Statistical analysis of resulting linear trend estimations from Toulon's undersampled tide gauge record.

	Mean (mm yr^{-1})	Std dev (mm yr^{-1})	Skewness	Kurtosis
No IB correction	1.73	1.33	−0.59	2.68
IB correction	0.25	0.85	−0.37	2.5
MOG2D correction	0.62	0.67	0.28	3.15

forcing). At this point two types of analysis could be carried out: 1) correcting for high frequency only (applying a high-pass filter to our models) in order to conserve the trend and the low-frequency atmospheric contribution for our estimation, or 2) correcting for the whole atmospheric signal in order to analyze the residual contributions associated with steric, water mass exchange and dynamical circulation contributions. It was the second choice that was carried out here. Re-

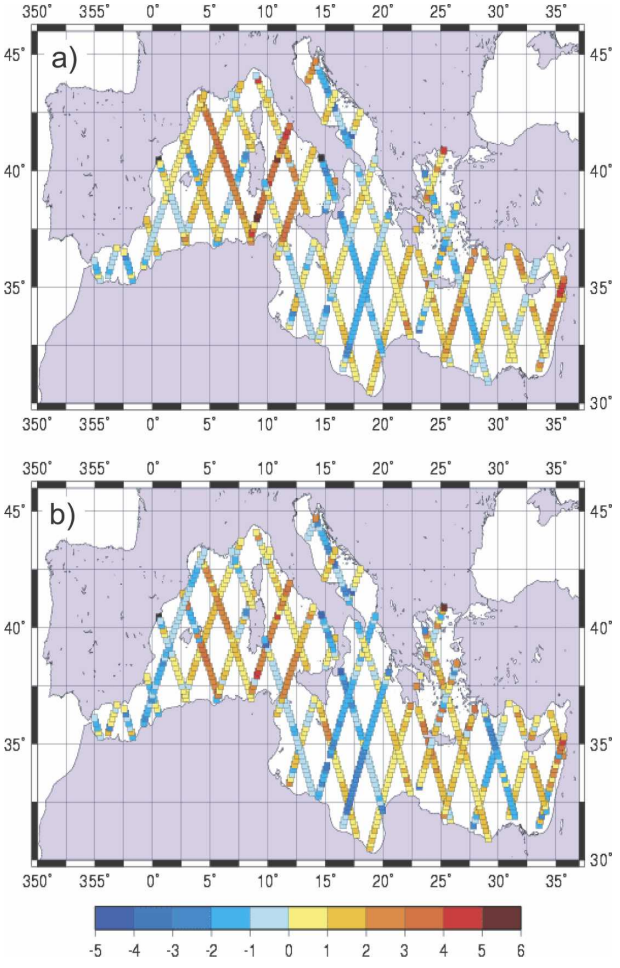

FIG. 6. Linear trend correction (mm yr^{-1}) on the 1993–2002 period associated with (a) the IB correction and (b) the MOG2D correction.

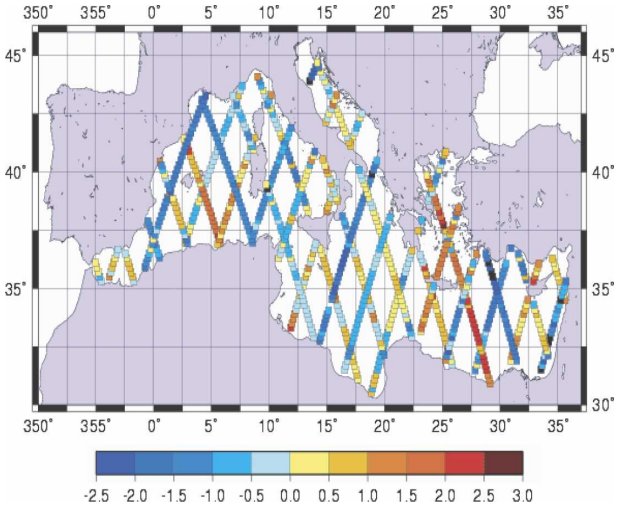

FIG. 7. Linear trend correction differences (mm yr^{-1}) on the 1993–2002 period between the IB correction and the MOG2D correction.

sulting corrections are shown in Fig. 6. Applying the IB correction (Fig. 6a) will correct linear trend estimations by values ranging from -2 to 3 mm yr^{-1} (reaching ± 5 mm yr^{-1} at localized points), whereas MOG2D correction will be slightly higher with values ranging between -3 and 3 mm yr^{-1} (Fig. 6b). Notable correction differences can be observed between one track and another, even at crossing points. This comes from a phase effect. Effectively the high magnitude of these corrections is a result of an aliasing effect dependent on the phase of the samplings, as shown in Fig. 5. Each track corresponds to a different crossing time and a notable phase difference ensues from this, which explains this behavior.

Moreover, applying the IB correction rather than the MOG2D model-derived correction can also be compared by computing $\delta\hat{T}_{\text{wind}}$, the difference between the respective linear trend corrections (Fig. 7). The correction choice can have considerable effects on linear trends estimations ranging between -2.5 and 3 mm yr^{-1}, showing that the wind action and also the dynamical response to surface pressure and wind stress have a strong contribution that the IB model is not able to take into account.

The magnitude of the sea level linear trends strongly depends on the period length considered as was already noted by Tsimplis and Spencer (1997) over a longer period. The mean maximum magnitude (in absolute value) $\overline{\chi}_\alpha$ of linear trend is represented as a function of the windows length L in Fig. 8a.

For a 3-yr length period, linear trends (in absolute values) can reach locally 60 mm yr^{-1}, with a mean maximum exceeding 30 mm yr^{-1}. When considering a 9-yr length period, maximum linear trends do not exceed 35 mm yr^{-1} and their mean maximum does not exceed 12 mm yr^{-1}.

In terms of mean maximum magnitude of the linear trend correction—let us call it $\overline{\chi}_{\delta\alpha}$—a similar behavior can be expected (Fig. 8b). Using the most efficient corrections (MOG2D model-derived correction in our case), the magnitude of the mean maximum correction will vary from 12 mm yr^{-1} for a 3-yr time span considered to 2 mm yr^{-1} for a 9-yr time span. Using the IB correction the mean maximum corrections are slightly smaller (from 10 to 1.8 mm yr^{-1}, respectively). This clearly highlights the necessity to take into account the window length when comparing two linear trends estimations, and also underlines the risks in rudely extrapolating a linear trend estimated over a given period to a longer time scale.

Last, linear trend corrections associated with the MOG2D correction rather than the IB correction have mean maximum values varying from 7 mm yr^{-1} for a 3-yr length window to 1.8 mm yr^{-1} for 9 yr. This underlines the usefulness of pressure- and wind-driven corrections for a more precise linear trend estimation.

4. Conclusions

SLE variations observed in the Mediterranean Sea show strong spatial contrasts when considering the whole basin at interannual time scales. The linear trends have been estimated at a local scale along the altimetric tracks. Over a 9-yr time span, their magnitudes vary between -24 and 29 mm yr^{-1}, which is in agreement with larger-scale observations from previous authors over shorter time periods. For more precise local linear trend estimation, it is required to correct SLE for atmospheric loading (surface pressure and wind stress) due to the T/P aliasing effect (and for any other mission—for example, *Jason-1*—that samples in a similar manner).

Corrections associated with this effect easily reach 2 mm yr^{-1} over a 9-yr period, but are much more important over shorter periods (reaching 12 mm yr^{-1} for a 3-yr time span). Applying the IB correction allows the calculation of substantially better linear trend estimations. However the MOG2D correction clearly leads to a more precise estimation because it allows wind action to be taken into account and a dynamical and nonlinear response. Taking into account these two processes can affect the corrections by more than 1.8 mm yr^{-1} over a 9-yr period, and up to 7 mm yr^{-1} over a 3-yr period. Several improvements can be added to our trend estimations by reducing signal noise through better data selection, by using a more adapted mean sea surface

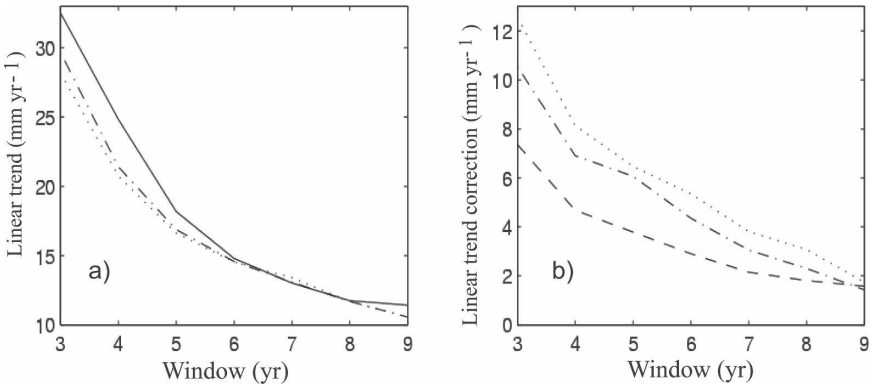

FIG. 8. (a) Mean maximum linear trend (mm yr^{-1}) in SLE vs time series length (yr): with no correction applied (solid line), with IB correction applied (dashed–dotted line), and with MOG2D correction applied (dotted line). (b) Linear trend correction in SLE (mm yr^{-1}) vs the time series length (yr): IB correction (dashed–dotted line), MOG2D correction (dotted line), and the MOG2D minus IB linear trend correction difference (dashed line).

estimation and using a more efficient tide estimation. For instance, the tidal correction has been taken from FES99, which was optimized for the global ocean tides. Improved tidal corrections could be obtained from regionally optimized tidal models such as a MOG2D based model developed for the Mediterranean Sea and shelf seas. Concerning the interaction at the Gibraltar Strait, although the Atlantic Ocean has only a minor influence on the Mediterranean Sea via this strait, experiments have demonstrated that the impact of the boundary conditions realism was significant for the model simulations' accuracy (F. Lyard, unpublished manuscript). For future analysis, signal noise reduction influence based on a comparison between *Jason-1* data with T/P data may also be investigated.

Acknowledgments. We thank R. Morrow, P. Mazzega, and C. Cabanes for useful discussions. Support from CLS, CNES, and CNRS in France is also gratefully acknowledged. Anonymous reviewers are also gratefully acknowledged for their constructive comments.

APPENDIX A

Instrumental corrections C_{TMR} are applied as follows:

$$C_{\mathrm{TMR}}(t) = \begin{cases} -1.2(t - 1993) & \text{for } 1993 \le t < 1997 \\ -4.8 & \text{for } t \ge 1997 \end{cases} \tag{A1}$$

to compensate for the microwave radiometer bias (Haines and Bar-Sever 1998). A 7-mm bias is also applied to account for the switch from altimeter side A from the beginning of 1999 (cycle number 236) to its redundant side B (Mitchum 2000):

$$C_{\mathrm{alti}}(t) = \begin{cases} 0.0 & \text{for } 1993 \le t < 1999.11 \\ +7.0 & \text{for } t \ge 1999.11 \end{cases}. \tag{A2}$$

APPENDIX B

The along-track mean sea surface $M(\lambda, \varphi)$ is computed via the fitting of the third-degree polynomial surface on all the data available in a box of 0.2° of latitude with

$$M(\lambda, \varphi) = a_1\lambda + a_2\varphi + a_3\lambda^2 + a_4\varphi^2 + a_5\lambda\varphi + a_6\lambda^3 + a_7\varphi^3 + a_8\lambda^2\varphi + a_9\lambda\varphi^2, \tag{B1}$$

where λ and φ are the latitude and the longitude, respectively, and where the a_i are the fitted parameters (Mangiarotti 2003). This surface height is then subtracted from the initial data box providing three homogeneous dataset $\hat{h}_\gamma$ of sea level anomaly as follows:

$$\hat{h}_\gamma(t, \lambda, \varphi) = h_\gamma(t, \lambda, \varphi) - M(\lambda, \varphi). \tag{B2}$$

These anomalies are then spatially averaged in each box in order to provide 10-day macromeasurements time series $\overline{h}_\gamma$ of sea level anomalies:

$$\overline{h}_\gamma(t, \lambda, \varphi) = \frac{1}{N}\sum_{i=1}^{N} \hat{h}_\gamma(t, \lambda, \varphi) \quad \text{for} \quad \lambda \in [\lambda_n; \lambda_n + 0.2], \tag{B3}$$

where N is the number of measurements available for a given track in one box at one passage time.

APPENDIX C

Practically, T/P individual initial measurements have been randomly perturbed with white noise taken be-

tween ±5 cm [a value that is close to the standard error of 4.1 cm given for an individual measurement by Chelton et al. (2001)]. Two ensembles of perturbations have been computed for each time series and the error $\hat{\varepsilon}$ is estimated as the biggest absolute shift from $\hat{T}_\gamma$ the unperturbed linear trend estimation:

$$\hat{\varepsilon} = \max(|T_1 - \hat{T}_\gamma|, |T_2 - \hat{T}_\gamma|), \qquad \text{(C1)}$$

where T_1 and T_2 denote the linear trend estimates obtained from the perturbation sets. A classical formal error estimation would provide much lower (one order of magnitude lower, say around 0.1 mm yr^{-1}) but less robust values.

REFERENCES

Artegiani, A., D. Bregant, E. Paschini, N. Pinardi, F. Raicich, and A. Russo, 1997: The Adriatic Sea general circulation. Part I: Air–sea interactions and water mass structure. *J. Phys. Oceanogr.,* **27,** 1492–1514.

Ayoub, N., P.-Y. Le Traon, and P. De Mey, 1998: A description of the Mediterranean surface variable circulation from combined ERS-1 and Topex/Poseidon altimetric data. *J. Mar. Syst.,* **18,** 3–40.

Béthoux, J. P., and B. Gentili, 1999: Functioning of the Mediterranean Sea: Past and present changes related to freshwater input and climate changes. *J. Mar. Syst.,* **20,** 33–47.

——, ——, and D. Tailliez, 1990: Warming trend in the western Mediterranean deep water. *Nature,* **347,** 660–662.

——, ——, and ——, 1998: Warming and freshwater budget change in the Mediterranean since the 1940s, their possible relation to the greenhouse effect. *Geophys. Res. Lett.,* **25,** 1023–1026.

Carrère, L., 2004: Etude et modélisation de la réponse hautes fréquences de l'océan global aux forçages météorologiques. Ph.D. thesis, Université Toulouse III, Paul Sabatier, 313 pp.

——, and F. Lyard, 2003: Modeling the barotropic response of the global ocean to atmospheric wind and pressure forcing—Comparisons with observations. *Geophys. Res. Lett.,* **30,** 1275, doi:10.1029/2002GL016473.

Cartwright, D. E., and R. J. Tayler, 1971: New computations of the tide-generating potential. *Geophys. J. Roy. Astron. Soc.,* **23,** 45–74.

——, and A. C. Edden, 1973: Corrected tables of tidal harmonics. *Geophys. J. Roy. Astron. Soc.,* **33,** 253–264.

Cazenave, A., C. Cabanes, K. Dominh, and S. Mangiarotti, 2001: Recent sea level change in the Mediterranean Sea revealed by Topex/Poseidon satellite altimetry. *Geophys. Res. Lett.,* **28,** 1607–1710.

Chelton, D. B., J. C. Ries, B. J. Haines, L.-L. Fu, and P. Callahan, 2001: Satellite altimetry. *Satellite Altimetry and Earth Science,* L.-L. Fu and A. Cazenave, Eds., Academic Press, 1–131.

Ducet, N., P. Y. Le Traon, and P. Gauzelin, 1999: Response of the Black Sea mean level to atmospheric pressure and wind forcing. *J. Mar. Syst.,* **22,** 311–327.

Eanes, R. J., and S. V. Bettadpur, 1995: The CSR 3.0 global ocean tide model. Tech. Memo. CSR-TM-95-06, Center for Space Research, University of Texas at Austin.

Fenoglio-Marc, L., 2002: Long-term sea level change in the Mediterranean Sea from multi-satellite altimetry and tide gauges. *Phys. Chem. Earth,* **27,** 1419–1431.

Fu, L. L., and G. Pihos, 1994: Determining the response of sea level to atmospheric pressure forcing using TOPEX/POSEIDON data. *J. Geophys. Res.,* **99,** 24 633–24 642.

Garrett, C., 1983: Variable sea level and strait flow in the Mediterranean: A theoretical study of the response to meteorological forcing. *Oceanol. Acta,* **6,** 79–87.

Gaspar, P., F. Ogor, P.-Y. Le Traon, and O.-Z. Zanife, 1994: Estimating the sea state bias of the Topex and Poseidon altimeters from crossover differences. *J. Geophys. Res.,* **99** (C12), 24 981–24 994.

Haines, B. J., and Y. E. Bar-Sever, 1998: Monitoring the TOPEX microwave radiometer with GPS: Stability of columnar water vapor measurements. *Geophys. Res. Lett.,* **25,** 3563–3566.

Hellereman, S., and M. Rosenstein, 1983: Normal wind stress over the World Ocean with error estimates. *J. Phys. Oceanogr.,* **13,** 1093–1105.

Hirose, N., I. Fukumori, and V. Zlotnicki, 2001: Modeling the high-frequency barotropic response of the ocean to atmospheric disturbances: Sensitivity to forcing, topography, and friction. *J. Geophys. Res.,* **106** (C12), 30 987–30 995.

Larnicol, G., N. Ayoub, and P.-Y. Le Traon, 2002: Major changes in Mediterranean Sea level variability from 7 years of Topex/Poseidon and ERS-1/2 data. *J. Mar. Syst.,* **33–34,** 63–89.

Lefèvre, F., 2000: Modélisation des marées océaniques à l'échelle globale: Assimilation de données in situ et altimétriques. Ph.D. thesis, Université Toulouse III, Paul Sabatier, 280 pp.

Le Provost, C., 2001: Ocean tides. *Satellite Altimetry and Earth Sciences: A Handbook of Techniques and Applications,* L.-L. Fu and A. Cazenave, Eds., International Geophysical Series, Vol. 69, Academic Press, 267–303.

Lynch, D. R., and W. G. Gray, 1979: A wave equation model for finite element tidal computations. *Comput. Fluids,* **7,** 207–228.

Mangiarotti, S., 2003: Les variations basse fréquence du niveau de la mer au cours de la deuxième moitié du XX^{ème} siècle par altimétrie spatiale et marégraphie. Ph.D. thesis, Université Toulouse III, Paul Sabatier, 178 pp.

Mitchum, G. T., 2000: An improved calibration of satellite altimetric heights using tide gauge sea levels with adjustment for land motion. *Mar. Geod.,* **23,** 145–166.

Pinardi, N., and E. Masetti, 2000: Variability of the large scale general circulation of the Mediterranean Sea from observations and modelling: A review. *Palaeogeogr. Palaeoclimatol. Palaeoecol.,* **158,** 153–174.

Ross, T., C. Garrett, and P.-Y. Le Traon, 2000: Western Mediterranean sea-level rise: Changing exchange flow through the Strait of Gibraltar. *Geophys. Res. Lett.,* **27,** 2949–2952.

Tapley, B. D., and Coauthors, 1996: The joint gravity model 3. *J. Geophys. Res.,* **101** (B12), 28 029–28 049.

Tsimplis, M. N., and G. N. Vlahakis, 1994: Meteorological forcing and sea-level variability in the Aegean Sea. *J. Geophys. Res.,* **99** (C5), 9879–9890.

——, and N. E. Spencer, 1997: Collection and analysis of monthly mean sea level data in the Mediterranean and the Black Sea. *J. Coastal Res.,* **13,** 534–544.

——, and T. F. Baker, 2000: Sea level drop in the Mediterranean Sea: An indicator of deep water salinity and temperature changes? *Geophys. Res. Lett.,* **27,** 1731–1734.

——, S. A. Josey, M. Rixen, and E. V. Stanev, 2004: On the forcing of sea level in the Black Sea. *J. Geophys. Res.,* **109,** C08015, doi:10.1029/2003JC002185.

Wahr, J. M., 1985: Deformation induced by polar motion. *J. Geophys. Res.,* **90** (B11), 9363–9368.